Theor Chem Acc (2016) 135:258
DOI 10.1007/s00214-016-2017-3

REGULAR ARTICLE

Study on the structures and properties of praseodymium-doped silicon clusters $PrSi_n$ (n = 3–9) and their anions with density functional schemes

Yutong Feng[1] · Jucai Yang[1,2] · Yuming Liu[2]

Received: 24 June 2016 / Accepted: 25 October 2016 / Published online: 2 November 2016

Abstract The equilibrium geometries and properties such as adiabatic electron affinities (AEAs), simulated photoelectron spectra (PES), dissociation energies, relative stabilities, HOMO–LUMO gaps, charges transfer, and magnetic moments of $PrSi_n$ (n = 3–9) and their anions have been made a detailed study by means of the ABCluster global search technique combined with density functional methods. The structure optimization is carried out with three exchange correlation functionals (B3LYP, PBE0, and mPW2PLYP). The ground state structures predicted by mPW2PLYP are thought to be trustworthy. The experimental PES of $PrSi_4^-$ is reassigned in light of the theoretical results, and the experimental AEAs of 2.0 ± 0.1 eV are obtained. The mPW2PLYP AEAs of $PrSi_n$ are in excellent agreement with the experimental values. The average absolute deviations from experiment are only 0.05 eV, and the maximum deviations are 0.10 eV. The accordance between the experimental PES and the theoretical simulations indicates that the ground state structures of $PrSi_n^-$ (n = 4–9) are trustworthy. Doping Pr atom to Si_n (n = 3–9) clusters raises the photochemical sensitivity. A large proportion of the total magnetic moments for all of these species are contributed by Pr atom.

Keywords $PrSi_n$ · Ground state structures · Electron affinities · Charge transfer · Magnetic moment

✉ Jucai Yang
yangjc@imut.edu.cn

[1] School of Energy and Power Engineering, Inner Mongolia University of Technology, and Inner Mongolia Key Laboratory of Theoretical and Computational Chemistry Simulation, Hohhot 010051, People's Republic of China

[2] School of Chemical Engineering, Inner Mongolia University of Technology, Hohhot 010051, People's Republic of China

1 Introduction

Introducing rare earth (RE) metal atoms into semiconductor clusters in the past decade, especially silicon, has been a subject of greater interest in respect that doping RE atom into silicon clusters can alter significantly their structures, properties, and stabilities [1–20].

There have been some previous studies on introducing RE atoms into silicon clusters. Bowen et al. [1, 2] presented the PES of $RESi_n^-$ (RE = Eu, Sm, Yb, Pr, Gd, and Ho $3 \le n \le 17$) and found that they can be divided into two categories based on their appearance. The spectra of $EuSi_n$, $YbSi_n$, and $SmSi_n$ belong to group "A", and the spectra of $PrSi_n$, $GdSi_n$, and $HoSi_n$ fall into group "B". In the previous investigation [18–20], we found that the 4*f* electron of Eu, Yb, and Sm atoms in Si_n surrounding hardly participates in bonding. In this work, we can find that the 4*f* electron of Pr atoms participates in bonding. More specifically, a 4*f* electron of Pr atom removed to 5*d* orbital, and then the 5*d* electron participates in bonding. That is actually similar to Gd atom which itself contains a 5*d* electron; that is, the 4*f* or 5*d* electron of group "B" atom in the clusters prefers to take part in bonding. While for the group "A", the 4*f* electron hardly participates in bonding. On the aspect of the experiment, Nakajima et al. [3, 4] have firstly explored the $TbSi_n^-$, $LuSi_n^-$, and $HoSi_n^-$ ($6 \le n \le 20$) clusters by using PES. Urged by these experimental observations, some theoretical simulations have been achieved for $RESi_n$ clusters. The equilibrium geometries and properties such as relative stabilities, magnetic moments, charge transfers, HOMO–LUMO gaps, and adiabatic electron affinities (AEAs) of neutral $SmSi_n$ and $YbSi_n$ ($n \le 13$) and their charged ions were calculated by using various density functional theory (DFT) methods [8–12]. The growth behavior of the ground state structures for $LuSi_n$, $HoSi_n$, $LaSi_n$, and $GdSi_n$ ($n \le 21$)

was also investigated by means of DFT schemes [13–17]. Recently, we evaluated the ground state structures and electron affinities of $SmSi_n$, $EuSi_n$, and $YbSi_n$ ($3 < n < 11$) and their anions by means of several DFT techniques including B3LYP, wB97X, PBE0, PBE, and B2PLYP and found that the theoretical AEAs calculated by these methods agree with the experimental values [18–20].

In this study, the ground state structures and properties including AEAs, relative stabilities, dissociation energies (DEs), simulated PES spectra, HOMO–LUMO gaps, charges transfers, and magnetic moments of neutral $PrSi_n$ ($n = 3$–9) and their anions are explored with the aim of understanding how their properties are different from that spectra belong to "A". The simulated PES spectra and calculated AEAs are compared with experimental ones in order to not only verify the reliability of the predicted results but also aid the reassignment of experimental PES. This work will also provide specific guidance for further investigation of medium-size clusters.

2 Theoretical methods

The calculations are carried out at the level of the DFT with the B3LYP [21, 22], PBE0 [23], and mPW2PLYP [24] functional. The basis sets used in the geometry optimization process are cc-pVTZ [25] for Si atoms and the segmented (SEG) Gaussian valence basis sets and relativistic small-core potentials (ECP28MWB) [26] (denoted as SEG/ECP) for Pr atoms. At the B3LYP and PBE0 levels, calculations of harmonic frequency for neutral $PrSi_n$ ($n = 3$–9) and their anions were done to assure that the optimized isomers are local minima. Then, the SEG basis sets of Pr were augmented by diffuse functions 2*pdfg* with exponents 0.028 and 0.015 (*p*), 0.032 (d), and 0.05 (*f, g*) [27] (denoted as aug-SEG/ECP), which aug-cc-pVTZ basis sets of Si [26] were used in the single-point energies calculations. Finally, the energies at 0 K are gained by adding the zero-point vibration energy (ZPVE) (the mPW2PLYP ZPVE employed that of the PBE0). The GAUSSIAN 09 codes [28] are used to perform all of the calculations.

The initial geometries are obtained by using the ABCluster global search method [29] combined with the GAUSSIAN 09 codes. The first step is achieved at the B3LYP level with relativistic large-core effective core potentials (ECP-53MWB) [30, 31] for Pr atoms and 6-31G basis set for Si atoms. More than 100 initial geometries of each $PrSi_n$ clusters are generated for $n \leq 7$, and more than 300 configurations are generated for $n \geq 8$. The second step, the top ten lowest energy structures from the first step, and those with their energy differences within 0.8 eV from the lowest energy structure, are selected and optimized again by means of the B3LYP with the SEG/ECP basis set for Pr and the cc-pVTZ basis sets for Si atoms. Finally, the structures from the second step with their energy differences within 0.8 eV are optimized by means of the remaining two methods. The "substitutional structure", which can be regarded as substituting a Si atom of the ground state structure of Si_{n+1} with a Pr atom, is also taken into account in respect that the ground state structures of $YbSi_n$, $SmSi_n$, and $EuSi_n$ are substitutional structure [18–20]. The global search, after all, is a mathematical scheme, and it is almost impossible to take an "ergodic" sampling on the potential energy surfaces for large clusters, especially for heteroatom clusters. Our experience is that, all of the "substitutional structures" are included when 100 configurations are generated from the ABCluster global search technique. However, starting from $n = 8$, only part of the "substitutional structures" are included when 300 (even up to 500) configurations are generated from the ABCluster global search method.

Furthermore, the spin multiplicities of quartet and sextuplet states were taken into account for neutral $PrSi_n$ ($n \leq 5$). And triplet and quintuplet state were considered for their anions. The results show that the quartet state is predicted to be the ground state structure for the neutral with the exception of PrSi which is sextuplet state. The ground state structure for anions $PrSi_n^-$ with $n = 1$–3 is calculated to be the quintuplet. The reason can be attributed to the ground state structure of Si_n with $n = 1$–3 is triplet electronic state. Starting from $n = 4$, the ground state structure is triplet electronic state. Although many isomers are obtained, the ground state structures are mainly presented.

3 Results and discussion

3.1 The ground state structures of $PrSi_n$ and their anions

The isomers optimized at the B3LYP, PBE0, and mPW-2PLYP levels are shown in Fig. 1 for $PrSi_n$ ($n = 3$–9) species and their anions. For $PrSi_3$, the ground state structure (shown in Fig. 1) is calculated to be an *approximate planar rhombus* with quartet electronic state, which is more stable than that of sextuplet by 0.77, 0.61, and 0.41 eV at the B3LYP, PBE0, and mPW2PLYP levels, respectively. For anion, the *approximate planar rhombus* **$PrSi_3^-$-I** (see Fig. 1) of triplet electronic state is more stable than that of **$PrSi_3^-$-II** isomer (see Fig. 1) by 0.39 and 0.01 eV at the B3LYP and PBE0 level, respectively. It is noted that for **$PrSi_3^-$-I**, the spin contamination occurs at the B3LYP and PBE0 levels due to the expectation value [2.69 (B3LYP) and 2.71 (PBE0)] of the total spin (S^2) as can be seen from Table 1. At the mPW2PLYP level, the *trigonal pyramid* **$PrSi_3^-$-II** of quintuplet electronic state is evaluated to be the ground state structure. It is more stable than that of **$PrSi_3^-$-I** by 0.15 eV in energy.

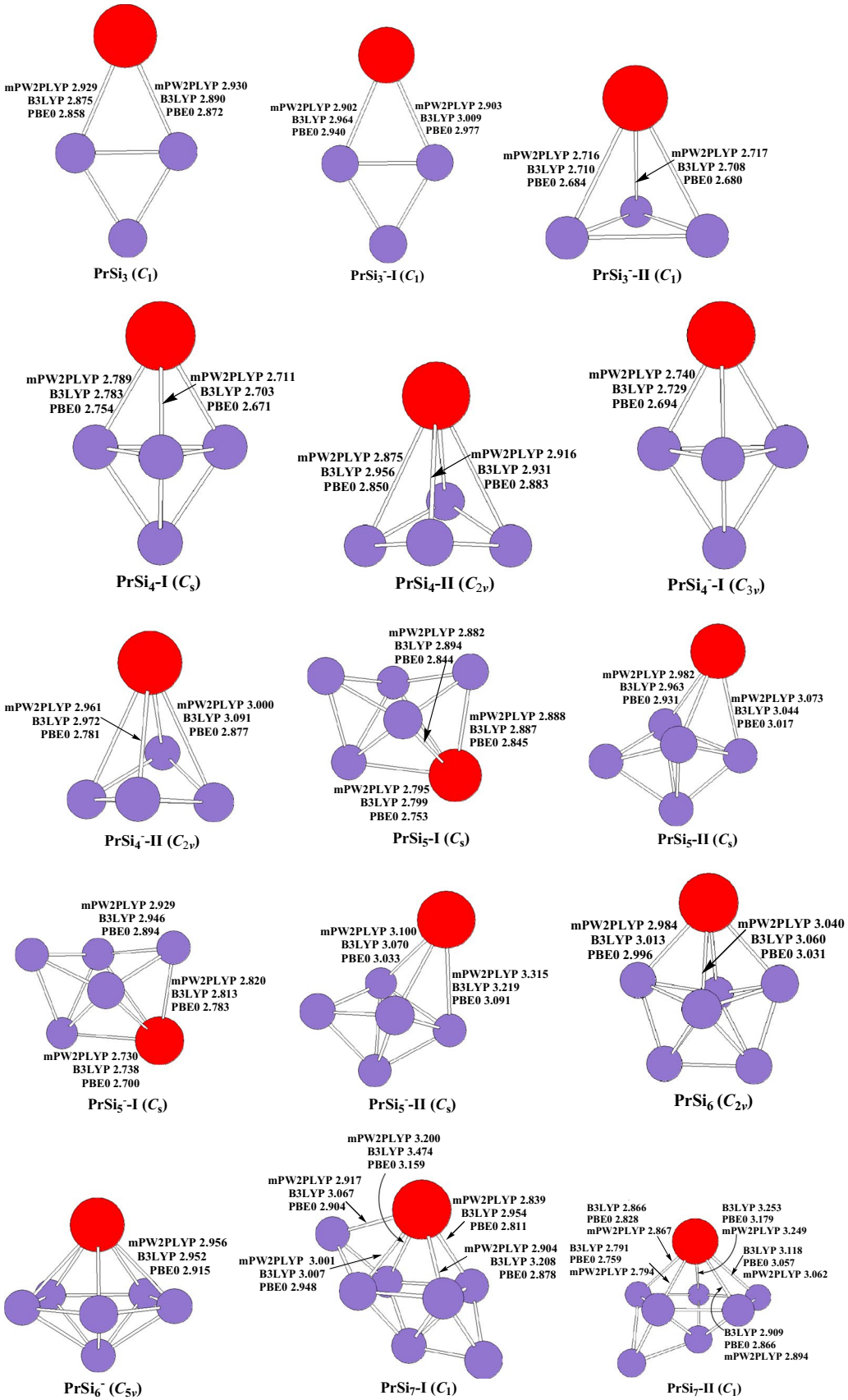

Fig. 1 Geometries of $PrSi_n$ ($n = 3$–9) and their anions in which *red color* (online) is Pr atom. The Pr–Si bond lengths are shown in Å

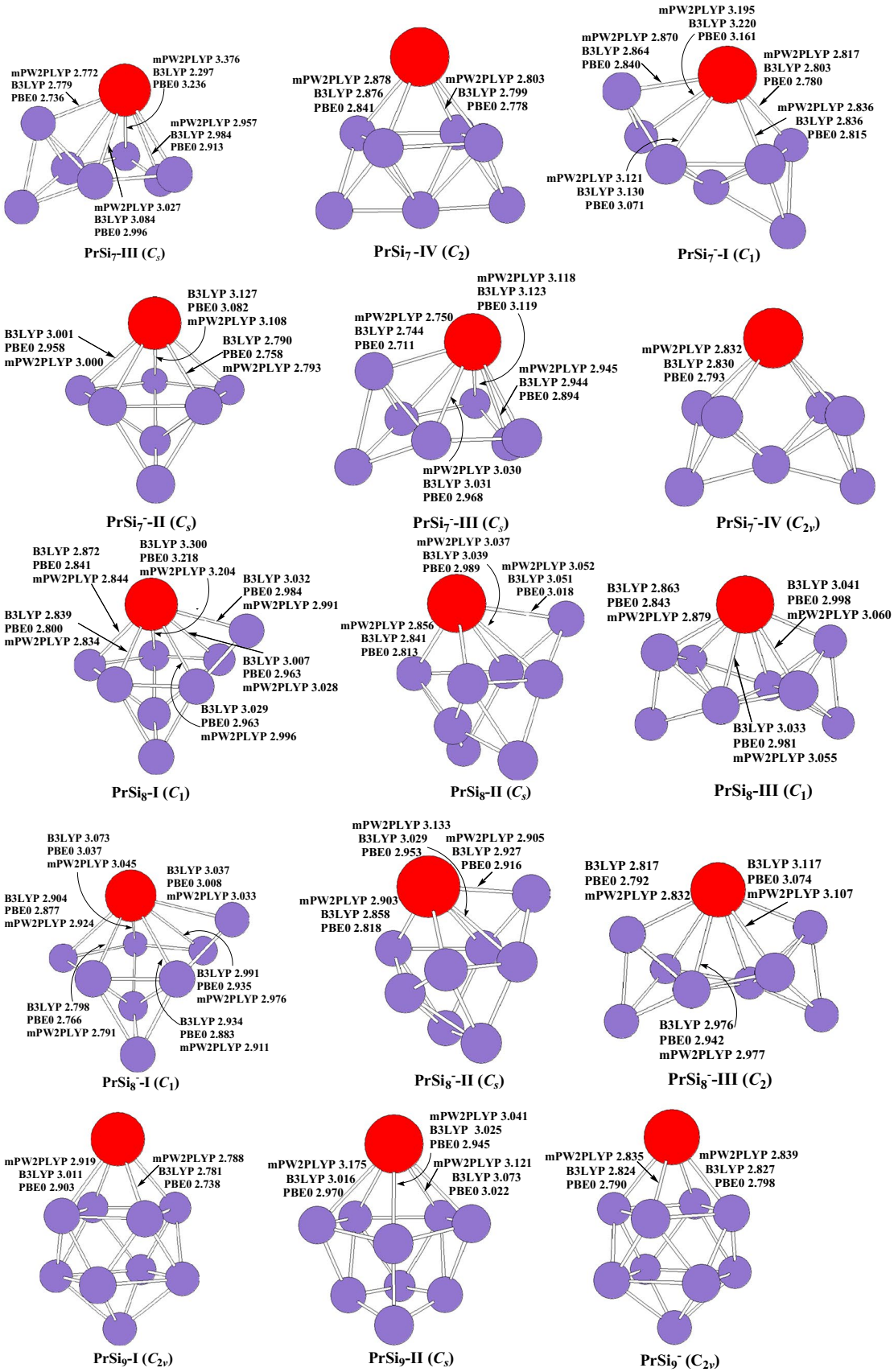

Fig. 1 continued

Table 1 Spin (S) and S^2 operator of $PrSi_n$ ($n = 3$–9) and their anions

Isomer	S	B3LYP S^2	PBE0 S^2	mPW2PLYP S^2
$PrSi_3$	3/2	3.76	3.76	3.76
$PrSi_3^-$I	2/2	2.69	2.71	2.15
$PrSi_3^-$II	4/2	6.04	6.05	6.10
$PrSi_4$-I	3/2	3.78	3.79	3.81
$PrSi_4$-II	3/2	4.13	3.86	3.82
$PrSi_4^-$I	2/2	2.02	2.02	2.02
$PrSi_4^-$II	2/2	3.30	2.04	3.05
$PrSi_5$-I	3/2	3.77	3.78	3.78
$PrSi_5$-II	3/2	3.76	3.76	3.76
$PrSi_5^-$I	2/2	2.12	2.04	2.03
$PrSi_5^-$-II	2/2	2.99	2.96	3.01
$PrSi_6$	3/2	3.76	3.76	3.76
$PrSi_6^-$	2/2	2.03	2.02	2.01
$PrSi_7$-I	3/2	3.76	3.79	3.81
$PrSi_7$-II	3/2	3.78	3.78	3.81
$PrSi_7$-III	3/2	3.77	3.79	3.84
$PrSi_7$-IV	3/2	3.80	3.78	3.79
$PrSi_7^-$I	2/2	2.02	2.02	2.02
$PrSi_7^-$II	2/2	2.04	2.02	2.01
$PrSi_7^-$III	2/2	2.03	2.01	2.01
$PrSi_7^-$-IV	2/2	2.02	2.01	2.01
$PrSi_8$-I	3/2	3.78	3.78	3.82
$PrSi_8$-II	3/2	3.77	3.77	3.78
$PrSi_8$-III	3/2	3.77	3.77	3.80
$PrSi_8^-$I	2/2	2.04	2.02	2.02
$PrSi_8^-$II	2/2	2.04	2.01	2.01
$PrSi_8^-$III	2/2	2.02	2.02	2.01
$PrSi_9$-I	3/2	3.77	3.78	3.81
$PrSi_9$-II	3/2	3.76	3.77	3.76
$PrSi_9^-$	2/2	2.03	2.02	2.01

For neutral $PrSi_4$, two isomers which compete with each other for the ground state structure are reported. The C_s-symmetry *trigonal bipyramind* **$PrSi_4$-I** of $^4A''$ electronic state, and the C_{2v}-symmetry **$PrSi_4$-II** of $^4A_1$ electronic state are shown in Fig. 1. The energy differences between **$PrSi_4$-I** and **$PrSi_4$-II** are only 0.07, 0.01, and −0.02 eV at the B3LYP, PBE0, and mPW2PLYP levels, respectively. For anion $PrSi_4^-$, the *trigonal bipyramind* **$PrSi_4^-$-I** with triplet electronic state (approximately C_{3v}-symmetry) is calculated to be the ground state structure. The C_{2v}-symmetry **$PrSi_4^-$-II** of $^3A_1$ electronic state is less stable in energy than that of **$PrSi_4^-$-I** by 0.56, 0.54, and 0.80 eV at the B3LYP, PBE0, and mPW2PLYP levels, respectively. Furthermore, the **$PrSi_4^-$-II** is spin contamination at the B3LYP and mPW2PLYP levels. Their quintuplet isomers are less stable in energy than the ground state structure **$PrSi_4^-$-I**. For example, the C_{2v}-symmetry isomer of $^5A_1$ electronic state, analogous to **$PrSi_4^-$-II** (not shown in Fig. 1), is less stable than the ground state **$PrSi_4^-$-I** structure by 0.48, 0.60, and 0.74 eV at the B3LYP, PBE0, and mPW2PLYP levels, respectively.

Two *face-capped trigonal bipyramind* with C_s-symmetry for neutral $PrSi_5$ is presented. At the mPW2PLYP level, the **$PrSi_5$-I** of $^4A'$ electronic state is predicted to be the ground state structure, which is more stable than the **$PrSi_5$-II** of $^4A''$ by 0.17 eV. While at the B3LYP and PBE0 levels, the **$PrSi_5$-II** isomer, analogous to the ground state structure of $YbSi_5$, $SmSi_5$, and $EuSi_5$ [18–20], is more stable in energy than that of **$PrSi_5$-I** by 0.33 and 0.23 eV, respectively. For anion, the isomer **$PrSi_5^-$-I** of $^3A'$ electronic state is predicted to be the ground state structure, which is more stable than the **$PrSi_5^-$-II** by 0.10, 0.30, and 0.70 eV at the B3LYP, PBE0, and mPW2PLYP levels, respectively. In addition, the **$PrSi_5^-$-II** is spin contamination at the B3LYP, PBE0, and mPW2PLYP levels.

Xu et al. [8] reported that the ground state structure of $PrSi_6$ and its anion is C_{2v}- and C_{5v}-symmetry *pentagonal bipyramid*, respectively. Our result is the same as their outcome.

For $PrSi_7$, four isomers are presented. The C_1-symmetry **$PrSi_7$-I** isomer which can be regarded as being derived from the *distorted bicapped octahedron* of Si_8 [32] by substituting a Si with a Pr atom is similar to the ground state structure of $EuSi_7$ [20], $SmSi_7$ [19], and $YbSi_7$ [18]. The approximate C_s-symmetry **$PrSi_7$-II** isomer is analogous to the most stable structure of $GdSi_7$ [17]. The isomers **$PrSi_7$-III** and **$PrSi_7$-IV** possess $^4A''$ and ^4A electronic state. At the mPW2PLYP and PBE0 levels, the **$PrSi_7$-II** structure is more stable in energy than those of **$PrSi_7$-I**, **$PrSi_7$-III**, and **$PrSi_7$-IV** by 0.05, 0.07, and 0.22 eV, and 0.05, 0.07, and 0.13 eV, respectively. At the B3LYP level, the **$PrSi_7$-I** structure is more stable in energy than the isomers of **$PrSi_7$-II**, **$PrSi_7$-III**, and **$PrSi_7$-IV** by 0.05, 0.01, and 0.27 eV, respectively. The energies of **$PrSi_7$-I**, **$PrSi_7$-II** and **$PrSi_7$-III** isomers are almost equal. Their energy differences fall in 0.07 eV. These indicate that the potential energy surface of $PrSi_7$ is flat and that accurate prediction of structures requires advanced quantum mechanical investigations. For anion $PrSi_7^-$, four isomers are also reported. At the mPW2PLYP level, the energies of **$PrSi_7^-$-II** structure of $^3A'$, **$PrSi_7^-$-III** of $^3A'$, and **$PrSi_7^-$-IV** of $^3A_2$ are nearly equal. The energy differences among them are within 0.02 eV. The **$PrSi_7^-$-I** isomer is less stable than that of **$PrSi_7^-$-III** by 0.07 eV in energy. At the B3LYP level, the **$PrSi_7^-$-IV** structure is more stable in energy than the isomers of **$PrSi_7^-$-I**, **$PrSi_7^-$-II**, and **$PrSi_7^-$-III** by 0.10, 0.05, and 0.08 eV, respectively. At the PBE0 level, the **$PrSi_7^-$-II** structure is more stable in energy than those of **$PrSi_7^-$-I**, **$PrSi_7^-$-III**, and **$PrSi_7^-$-IV** by 0.18, 0.09, and 0.04 eV in

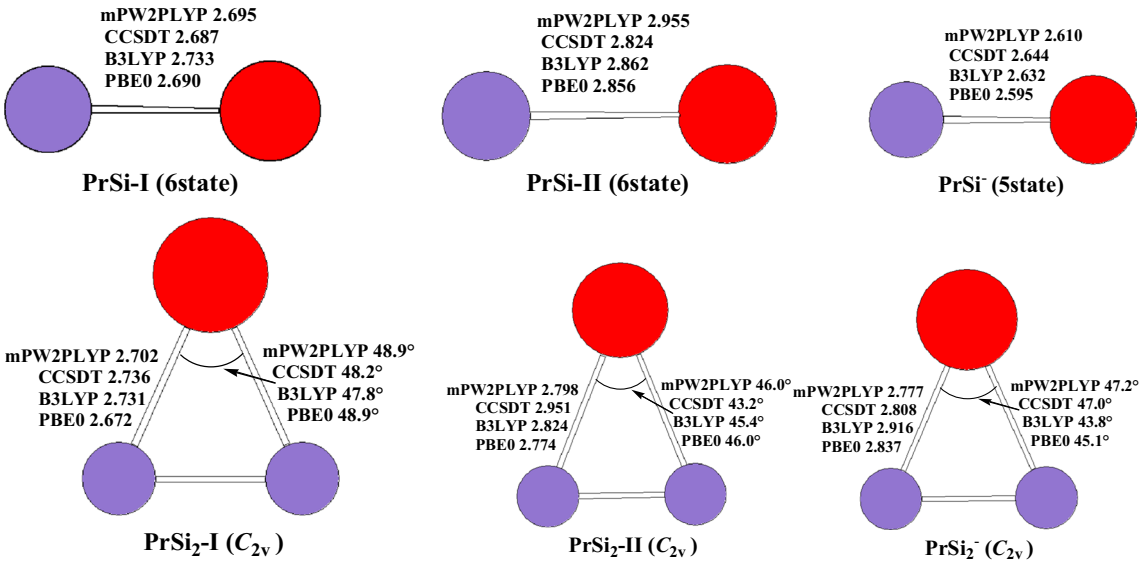

Fig. 2 Ground state structures for PrSi, $PrSi_2$, and their anions

energy, respectively. Although the energies of **$PrSi_7^-$-II**, **$PrSi_7^-$-III**, and **$PrSi_7^-$-IV** isomers are almost degenerated, the **$PrSi_7^-$-III** structures are assigned to the ground state structure based on the following fact: Compared to experimental PES, the simulated PES of **$PrSi_7^-$-III** is more consistent than that of **$PrSi_7^-$-II** and **$PrSi_7^-$-IV** (see Sect. 3.3).

For $PrSi_8$, three isomers are presented. The C_1-symmetry **$PrSi_8$-I** geometry is predicted to be the ground state structure at the B3LYP, PBE0, and mPW2PLYP levels. This result differs from those of $YbSi_8$, $SmSi_8$, and $EuSi_8$, of which ground state structure is the C_{2v}-symmetry *bicapped pentagonal bipyramid* [18–20]. The **$PrSi_8$-II** of $^4A''$ electronic state and *co-apex trigonal bipyramind* **$PrSi_8$-III** is less stable in energy than that of **$PrSi_8$-I** by 0.22, 0.25, and 0.03 eV, and 0.22, 0.25, and 0.26 eV, respectively. For anion, three isomers are also presented. The C_2-symmetry *co-apex trigonal bipyramind* **$PrSi_8^-$-III** of ^3A state is predicted to be the ground state structure. Energetically, it is more stable than the **$PrSi_8^-$-I** and **$PrSi_8^-$-II** by 0.34, 0.33, and 0.25 eV, and 0.17, 0.22, and 0.04 eV at the B3LYP, PBE0, and mPW2PLYP levels, respectively. The ground state structure of $PrSi_8^-$ differs from that of $YbSi_8^-$, $SmSi_8^-$, and $EuSi_8^-$, which is substitutional structure with C_{2v}-symmetry [18–20].

For $PrSi_9$, two geometries are presented. The C_{2v}-symmetry *bicapped antitetragonal prism* of $^4A_1$ state, **$PrSi_9$-I**, is predicted to be the ground state structure at the mPW2PLYP level. It is more stable than the **$PrSi_9$-II** isomer of $^4A''$ electronic state by 0.26 eV in energy. At the B3LYP and PBE0 levels, the **$PrSi_9$-II** isomer, analogous to the ground state structure of $GdSi_9$, $YbSi_9$, $SmSi_9$, and $EuSi_9$ [17–20], is calculated to be the most stable structure. It is more stable than that of **$PrSi_9$-I** by 0.37 and 0.25 eV, respectively. For anion $PrSi_9^-$, the C_{2v}-symmetry *bicapped antitetragonal prism* of $^3B_2$ electronic state is predicted to be the ground state at the B3LYP, PBE0, and mPW2PLYP levels. It is, again, different from that of $YbSi_9^-$, $SmSi_9^-$, and $EuSi_9^-$, of which ground state structure is substitutional structure with C_{3v}-symmetry [18–20].

From discussion above, we can conclude that (1) the functional dependence on the evaluated the ground state structure is seen for $PrSi_3^-$, $PrSi_5^-$, $PrSi_7^-$, $PrSi_7^-$, and $PrSi_9^-$. The mPW2PLYP scheme can be trustworthy based on the following fact: (1) The CCSD(T) method was adopted for geometry optimization of $PrSi_n$ (n = 1–2) and its anion in order to check reliability of methods (The geometries are shown in Fig. 2 and the total energies are listed in Table 2). From Table 1, we can see that the ground state structures predicted by the mPW2PLYP scheme are the same as those evaluated by the CCSD(T) method, while the ground state structures of PrSi and $PrSi_2$ predicted by the B3LYP and PBE0 methods differ from those of CCSD(T). (2) The electron affinities predicted by the mPW2PLYP are excellent in agreement with those of experimental data (see Sect. 3.2). (3) The simulated PES of the ground state structure predicted by the mPW2PLYP scheme is in accord with the experimental PES (see Sect. 3.3). It is to say that the methods including perturbative correlation part are very important as the species including *f*-electron (or *d*-electron) participating in bonding are treated [It is noted that the 4*f* electrons of Pr atom participate in bonding (see Sect. 3.6)]. (2) The extra electron effects on the ground state structure is intense. The ground state structures for $PrSi_3$, $PrSi_6$, and $PrSi_8$ differ from those of their anions. For $PrSi_4$ and $PrSi_7$,

Table 2 Total energies (in Hartree) of PrSi, $PrSi_2$, and their anions calculated at the methods/(aug-SEG/ECP, aug-cc-pVTZ)//methods/(SEG/ECP, cc-pVTZ) levels

Structure	Spin multiplicity	Methods			
		CCSD(T)	mPW2PLYP	B3LYP	PBE0
PrSi-I	6	−804.40236	−805.73579	−806.42141	−806.15220
PrSi−II	6	−804.38374	−805.73452	−806.43824	−806.16770
$PrSi^-$	5	−804.45379	−805.78069	−806.47306	−806.20199
$PrSi_2$-I	4	−1093.51526	−1095.18282	−1095.98602	−1095.58639
$PrSi_2$-II	4	−1093.48461	−1095.17739	−1095.99880	−1095.59538
$PrSi_2^-$	5	−1093.56071	−1095.22537	−1096.04193	−1095.63801

Table 3 Adiabatic electron affinities (AEAs) (in eV) with zero-point corrected for $PrSi_n$ ($n = 3$–9)

Species	Method	AEAs	Species	Method	AEAs
$PrSi_3$	B3LYP	0.96	$PrSi_7$	B3LYP	2.31
(**$PrSi_3$-I** ← **$PrSi_3^-$-II**)	PBE0	1.25	(**$PrSi_7$-II** ← **$PrSi_7^-$-III**)	PBE0	2.28
	mPW2PLYP	1.50		mPW2PLYP	2.30
	Expt.	–		Expt.	2.4 ± 0.1
$PrSi_4$	B3LYP	2.00	$PrSi_8$	B3LYP	2.49
(**$PrSi_4$-I** ← **$PrSi_4^-$-I**)	PBE0	2.03	(**$PrSi_8$-I** ← **$PrSi_8^-$-III**)	PBE0	2.58
	mPW2PLYP	2.09		mPW2PLYP	2.50
	Expt.	2.0 ± 0.1[a]		Expt.	2.5 ± 0.2
$PrSi_5$	B3LYP	1.84	$PrSi_9$	B3LYP	2.68
(**$PrSi_5$-I** ← **$PrSi_5^-$-I**)	PBE0	1.89	(**$PrSi_9$-I** ← **$PrSi_9^-$-**)	PBE0	2.75
	mPW2PLYP	1.90		mPW2PLYP	2.86
	Expt.	1.9 ± 0.1		Expt.	2.8 ± 0.1
$PrSi_6$	B3LYP	1.51			
(**$PrSi_6$** ← **$PrSi_6^-$**)	PBE0	1.43			
	mPW2PLYP	2.08			
	Expt.	2.1 ± 0.1			

[a] We reassigned the photoelectron spectrum of $PrSi_4^-$ recorded with 266 nm (see Ref [1]) and obtained the experimental value of 2.0 ± 0.1 eV (see text)

the ground state structures are undetermined because their potential energy surfaces are flat. The ground state structures of $PrSi_5^-$ and $PrSi_9^-$ are unchanged compared to its neutrals. (3) Starting from $n = 7$, the ground state structures of $PrSi_n$ and their anions differ from those of $YbSi_n$, $SmSi_n$, and $EuSi_n$.

3.2 AEAs

The AEAs of $PrSi_n$ ($n = 3$–9) are calculated and listed in Table 3. From Table 3, we can see that the theoretical AEAs of $PrSi_4$ deviated from experimental values (1.6 ± 0.1 eV) [1] by 0.40, 0.43, and 0.49 eV at the B3LYP, PBE0, and mPW2PLYP levels, respectively. In fact, the PES of $PrSi_4^-$ recorded with 266 nm photons has a very small hump in low binding energy region before the first major peak, and Grubisic et al. assigned it as onset [1]. Based on the our calculated results, we reassigned the first major peak as being due of the transition from the ground state of the anion to the ground states of the neutral and obtained the experimental value of 2.0 ± 0.1 eV. The very small hump is probably because of the existence of low-lying isomers in the experiment. In this way, the average absolute deviations from experiment for $PrSi_n$ ($n = 4$–9) are by 0.15, 0.16, and 0.05 eV at the B3LYP, PBE0, and mPW2PLYP levels, respectively. The largest deviations are 0.59, 0.67, and 0.10 eV, respectively. That is, the mPW2PLYP theoretical AEAs are in excellent agreement with the experimental data taken from Ref. [1].

In order to probe the effect of spin–orbit coupling (SOC), the effect of SOC is calculated via single-point calculations using the mPW2PLYP geometries and segmented all-electron relativistic Sapporo-DKH3-TZP basis sets with all-diffuse functions (Sapporo-DKH3-TZP-all) for Pr and Si atoms [33, 34], and using Hartree–Fock method via the Douglas–Kroll–Hess Hamiltonian (both with and without spin–orbit corrections). The AEAs with SOC corrections for $PrSi_n$ ($n = 4$–9) are listed in Table 4. From Table 4, we can see that the average absolute deviations from experiment are by 0.15, 0.16, and 0.06 eV at the B3LYP, PBE0,

Table 4 Adiabatic electron affinities (AEAs) (in eV) with spin–orbit coupling corrected for $PrSi_n$ ($n = 4$–9)

Species	Method	AEAs	Species	Method	AEAs
$PrSi_4$	B3LYP	2.06	$PrSi_7$	B3LYP	2.32
(**$PrSi_4$-I** ← **$PrSi_4^-$-I**)	PBE0	2.09	(**$PrSi_7$-II** ← **$PrSi_7^-$-III**)	PBE0	2.29
	mPW2PLYP	2.15		mPW2PLYP	2.31
$PrSi_5$	B3LYP	1.88	$PrSi_8$	B3LYP	2.45
(**$PrSi_5$-I** ← **$PrSi_5^-$-I**)	PBE0	1.93	(**$PrSi_8$-I** ← **$PrSi_8^-$-III**)	PBE0	2.54
	mPW2PLYP	1.94		mPW2PLYP	2.46
$PrSi_6$	B3LYP	1.52	$PrSi_9$	B3LYP	2.67
(**$PrSi_6$** ← **$PrSi_6^-$**)	PBE0	1.44	(**$PrSi_9$-I** ← **$PrSi_9^-$-**)	PBE0	2.74
	mPW2PLYP	2.09		mPW2PLYP	2.85

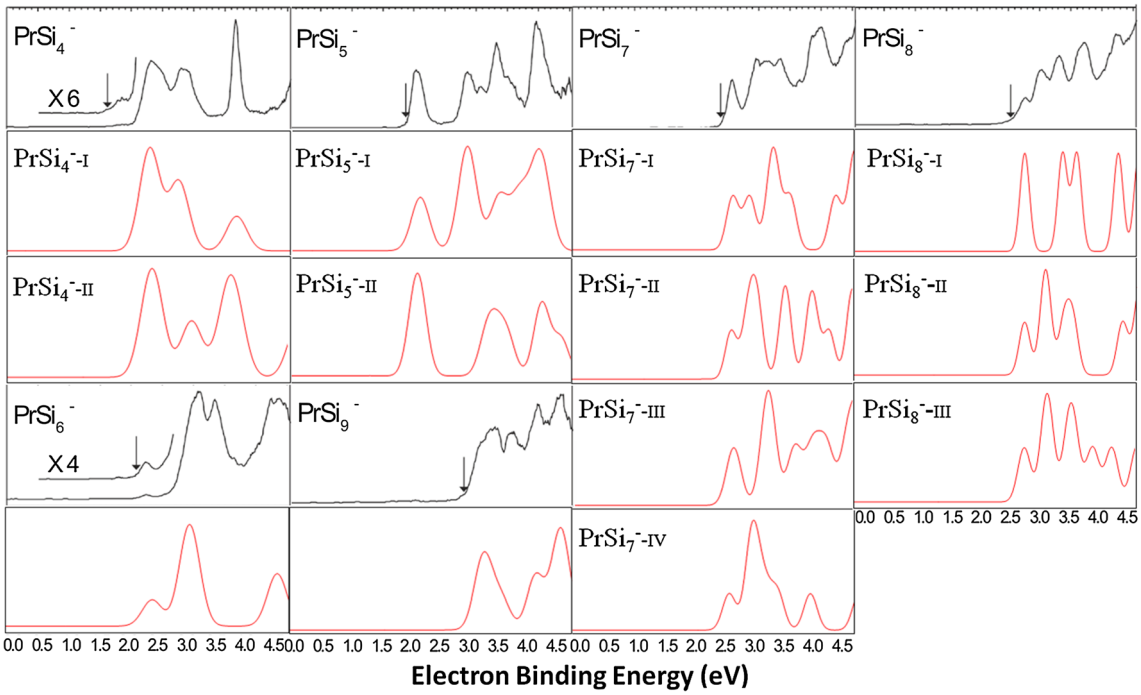

Fig. 3 Experimental photoelectron spectra (PES) (taken from Ref. [1], copyright 2009 American Society) and simulated PES at the mPW-2PLYP level for the anions $PrSi_n^-$

and mPW2PLYP levels, respectively. That is, the AEAs with SOC correction differ little from the results without SOC.

3.3 Simulated PES spectra

The anion PES spectra are simulated at the mPW2PLYP level on the basis of theoretically generalized Koopman theorem [35]. These simulated PES spectra and experimental ones taken from Ref. [1] are shown in Fig. 3. First step for the simulation is calculated the relative energies of the orbitals (ΔE_n) using the formula: $\Delta E_n = \Delta E_{\text{HOMO-}n} - E_{\text{HOMO}}$. Secondly, the first peak associated with the HOMO is placed at the VDE (vertical detachment energy) plot, and the peaks of the deeper orbitals are moved to higher binding energy. Thirdly, these peaks are suited with a unit-area Gaussian function of 0.20 eV FWHM (full widths at half maximum). To quantitatively compare theoretical intensities with experimental ones are not possible in respect that the nonadiabatic interactions and anharmonic resonances are not included in calculations. The locations and the amounts of distinct peaks of simulated PES for **$PrSi_4^-$-I**, **$PrSi_5^-$-I**, **$PrSi_7^-$-III** and **$PrSi_8^-$-III** in the range of ≤4.5 eV general accord with experimental ones as can be seen from Fig. 3. And the positions of the first two peaks of simulated PES of **$PrSi_6^-$** and **$PrSi_9^-$** are in accord with experimental ones. The agreement of locations and the amounts of distinct peaks between simulated and experimental PES reveals that the ground state structures of $PrSi_n^-$ ($n = 4$–9) reported in this paper are trustworthy.

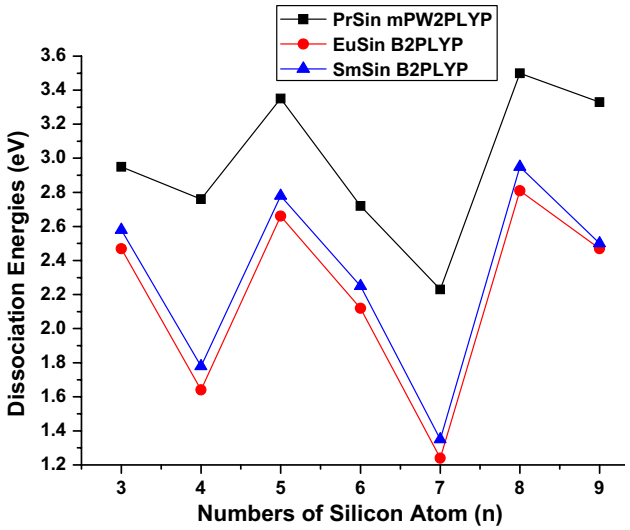

Fig. 4 Dissociation energy (in eV) of $PrSi_n$ with ZPVE corrections versus the number of atom n. The data of $SmSi_n$ and $EuSi_n$ ($n = 3$–9) are taken from Refs. [19, 20]

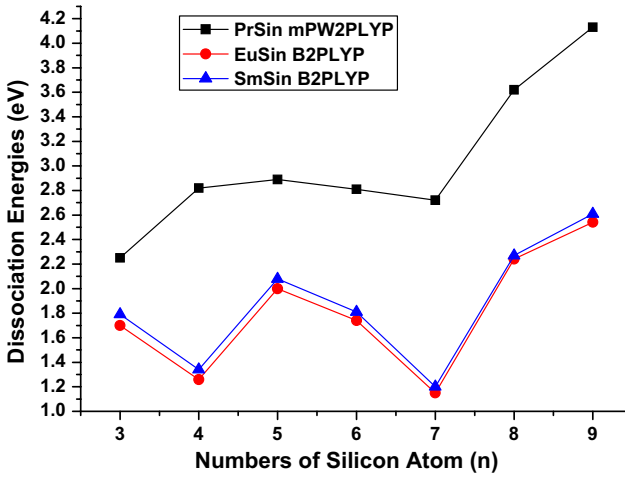

Fig. 5 Dissociation energy (in eV) of anion $PrSi_n^-$ with ZPVE corrections versus the number of atom n. The data of $SmSi_n^-$ and $EuSi_n^-$ ($n = 3$–9) are taken from Refs. [19, 20]

3.4 DEs

The DEs of $PrSi_n$ and their anions (defined as the energy required in the reactions $PrSi_n \rightarrow Pr + Si_n$ for neutral and $PrSi_n^- \rightarrow Pr + Si_n^-$ for anion) are calculated at the mPW-2PLYP level and drawn in Figs. 4 and 5, respectively. The DEs of $SmSi_n$ and $EuSi_n$ ($n = 3$–9) and their anions [19, 20] are also, respectively, shown in Figs. 4 and 5 in order to facilitate comparison. The higher values of the DEs show that the cluster bonding of a Pr atom is stable. As can be seen from Figs. 4 and 5, the DEs of $EuSi_n$ and $SmSi_n$ ($n = 3$–9) are smaller than that of $PrSi_n$. Although Pr atom has no $5d$ electrons, the $4f$ electron transfers to $5d$ orbital when Pr atom interacts with silicon clusters and then participates in bonding. The profiles of d-orbital are facilely deformed and tend to ionic polarization. The ionic bonding weakens, and the covalent bond strengthens due to the result of ionic polarization, and therefore causes a relatively large DE of $PrSi_n$. The same variation trends of DE curves exist on $PrSi_n$, $EuSi_n$, and $SmSi_n$. The DEs of $PrSi_4$ and $PrSi_7$ are local minima, and the DEs of $PrSi_5$ and $PrSi_8$ are local maxima. This result accords with that of ASi_n (A = Li, Na) and is interpreted by the parallelism between the EA and the DE of Si_n because the binding of an Pr to the Si_n species results in electronic charge transfer from the Pr atom to Si_n, similar to the conditions of binding of an alkali atom to the Si_n species [36]. The DEs of $EuSi_n^-$ and $SmSi_n^-$ ($n = 3$–9) are smaller than the DEs of $PrSi_n^-$. When $n = 4$–7, the DEs of $PrSi_n^-$ are different little from each other, but when $n = 8$ and 9, the DEs of $PrSi_n^-$ are larger than those of the others. The DEs of $PrSi_n^-$ are larger than those of corresponding neutral for $n = 7-9$, smaller for $n = 3$ and 5, and almost equal for $n = 4$ and 6. The explanation will be seen in Sect. 3.6.

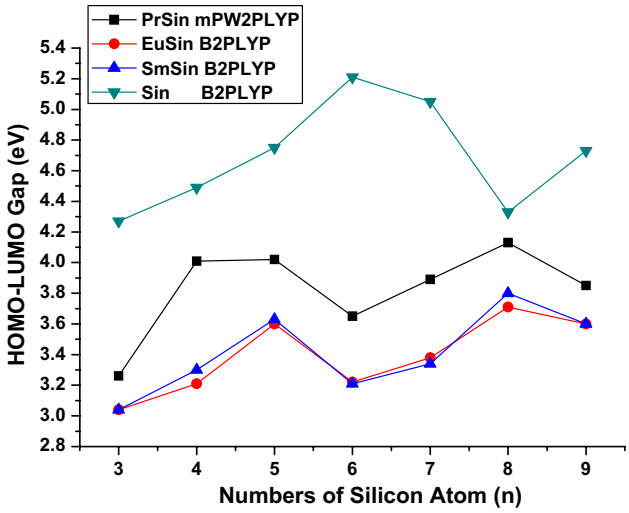

Fig. 6 HOMO–LUMO gaps (eV) of PrSin calculated at the mPW-2PLYP level. The HOMO–LUMO gaps of $SmSi_n$, $EuSi_n$, and Si_n are taken from Refs. [19, 20]

3.5 HOMO–LUMO gaps

HOMO–LUMO gaps can be served as an important criterion to reflect the chemical reactivity of molecules in a sense, especially for RE-doped silicon clusters which have fine photochemical sensitivity. The HOMO–LUMO gaps for the most stable structures of $PrSi_n$ ($n = 3-9$) predicted by the mPW-2PLYP method are tabulated in Fig. 6, along with the HOMO–LUMO gaps of $EuSi_n$, $SmSi_n$, and Si_n [19, 20] for comparison. From Fig. 6, we can conclude that similar to $EuSi_n$ and $SmSi_n$,

Table 5 Natural population analysis (NPA) valence configurations and charge of Pr atom (in a.u.) calculated with the mPW2PLYP scheme for the ground state structure $PrSi_n$ (n = 3–9) clusters and their anions

Species	Electron configuration	Charge
$PrSi_3$	[core]$6s^{0.27}4f^{2.93}5d^{0.62}6p^{0.06}$	1.13
$PrSi_4$	[core]$6s^{0.34}4f^{2.08}5d^{1.86}6p^{0.09}$	0.60
$PrSi_5$	[core]$6s^{0.36}4f^{2.07}5d^{1.83}6p^{0.13}$	0.65
$PrSi_6$	[core]$6s^{0.40}4f^{2.63}5d^{1.04}6p^{0.13}$	0.72
$PrSi_7$	[core]$6s^{0.34}4f^{2.07}5d^{1.94}6p^{0.19}$	0.23
$PrSi_8$	[core]$6s^{0.28}4f^{2.06}5d^{2.20}6p^{0.20}$	−0.06
$PrSi_9$	[core]$6s^{0.30}4f^{2.10}5d^{1.83}6p^{0.15}$	0.55
$PrSi_3^-$	[core]$6s^{0.46}4f^{2.08}5d^{2.33}6p^{0.08}$	0.00
$PrSi_4^-$	[core] $6s^{0.53}4f^{2.07}5d^{2.09}6p^{0.16}$	0.13
$PrSi_5^-$	[core]$6s^{0.32}4f^{2.09}5d^{2.19}6p^{0.05}$	0.29
$PrSi_6^-$	[core]$6s^{0.61}4f^{2.07}5d^{1.76}6p^{0.30}$	−0.04
$PrSi_7^-$	[core]$6s^{0.31}4f^{2.13}5d^{2.13}6p^{0.25}$	−0.05
$PrSi_8^-$	[core]$6s^{0.31}4f^{2.15}5d^{2.09}6p^{0.30}$	−0.02
$PrSi_9^-$	[core]$6s^{0.40}4f^{2.10}5d^{1.96}6p^{0.21}$	0.28

doping Pr atom to silicon species raises the photochemical sensitivity due to the fact that the HOMO–LUMO gap of $PrSi_n$ (n = 3–9) is smaller than that of Si_n with the same n. But the effect of raising photochemical sensitivity is not as good as the doping Eu or Sm to silicon species. The photochemical sensitivity of $PrSi_6$ is better than that of its neighboring clusters.

3.6 Charge transfer and magnetic moment

NPA (natural population analysis) is conducted with the mPW2PLYP method in order to further understand the interaction between the Pr atom and the Si_n species. The charges of Pr and NPA valence configurations are listed in Table 5. The magnetic moments of 6*s*, 4*f*, 5*d*, and 6*p* state for Pr, total magnetic moments of Pr, and total magnetic moments of the ground state of $PrSi_n$ (n = 3–9) and their anions are listed in Table 6. As can be seen from Table 5, the 4*f* shell of Pr in the cluster (except for $PrSi_3$) is obviously changed. The charge transfer occurs largely not only from 6*s* to 5*d* but also 4f to 5*d* orbitals, resulting in hybridization between the 6*s* and 5*d* orbitals. That is, the 4*f* electrons migrated to 5*d* orbit and then participated in bonding. The theoretical charges of the Pr in $PrSi_n$ (n = 3–9) species (except for $PrSi_8$) show that Pr atom acts as an electron donor and the characteristics of bonding between Pr and silicon clusters possess not only ionic bonds, but also covalent bonds in nature. Similar to anion $EuSi_n^-$ and $SmSi_n^-$ [19, 20], the majority of the additional electron's charge in $PrSi_n^-$ (n = 3–9) is found to be localized on the Si_n species. And average charges of 0.47 a.u. go back to Pr atom from Si_n compared to the neutral, which leads to decreasing of the ionic bond components and increasing of the covalent bond components. If the increased data are larger than the decreased data, the DEs of Pr from the $PrSi_n^-$ will be larger than those of their neutral (for example, $PrSi_7^-$, $PrSi_8^-$, and $PrSi_9^-$). For $PrSi_3^-$ and $PrSi_5^-$, the conditions are the opposite. And for $PrSi_4^-$ and $PrSi_6^-$, the increased and decreased value differs little from each other. From Table 6, we can see that the total magnetic moments of $PrSi_3$, $PrSi_5$, and $PrSi_n^-$ (n = 4–9) are contributed by Pr atom. And for the remaining species, in addition to a large proportion of magnetic moments that contributed by Pr atom, a small portion of magnetic moments are contributed by the silicon clusters.

Table 6 Magnetic moment (μ_B) of 6*s*, 4*f*, 5*d*, and 6*p* states for Pr atom, total magnetic moment (μ_B) of Pr atom, and total magnetic moment of the most stable structure of $PrSi_n$ (n = 3–9) and their anions calculated with the mPW2PLYP scheme

Species	Magnetic moment of Pr atom					Molecule
	6s	4f	5d	6p	Total	(μ_B)
$PrSi_3$	0.01	2.91	0.14	0.00	3.06	3
$PrSi_4$	0.01	1.98	0.36	0.01	2.36	3
$PrSi_5$	0.02	2.01	0.41	0.01	2.45	3
$PrSi_6$	0.24	2.55	0.16	0.04	2.99	3
$PrSi_7$	0.00	1.90	0.09	0.01	2.00	3
$PrSi_8$	0.00	1.96	0.31	0.00	2.27	3
$PrSi_9$	0.00	1.97	0.08	0.01	2.06	3
$PrSi_3^-$	0.02	1.98	0.97	0.01	2.98	4
$PrSi_4^-$	0.00	1.98	0.11	0.00	2.09	2
$PrSi_5^-$	0.00	1.98	0.03	0.08	2.09	2
$PrSi_6^-$	0.00	1.87	0.06	0.00	1.93	2
$PrSi_7^-$	0.00	1.91	0.08	0.00	1.99	2
$PrSi_8^-$	0.00	1.94	0.09	0.00	2.03	2
$PrSi_9^-$	0.00	1.97	0.08	0.00	2.05	2

4 Conclusions

We have investigated the equilibrium geometries and properties such as AEAs, simulated photoelectron spectra (PES), dissociation energies (DEs), relative stabilities, HOMO–LUMO gaps, charges transfer, and magnetic moments of $PrSi_n$ ($n = 3$–9) and their anions using the ABCluster global search technique combined with density functional methods. Prudently chosen DFT methods employed with aug-SEG/ECP basis set for Pr atoms are competent for the reliable prediction of the structures and properties of the $PrSi_n$ species. The mPW2PLYP results show that (1) starting from $n = 7$, the ground state structures of neutral $PrSi_n$ ($n = 3$–9) and their anions do not belong to "substitutional structure". When binding an electron to the ground state structure of the neutral, the extra electron effect on the ground state structure is intense. The ground state structures for $PrSi_3^-$, $PrSi_6^-$, and $PrSi_8^-$ are different from their neutral ones. (2) The experimental PES of $PrSi_4^-$ has been reassigned based on the theoretical results. Assigning experimental value of 2.0 ± 0.1 eV to the AEA is more justifiable than to 1.6 ± 0.1 eV. The mPW2PLYP AEAs of $PrSi_n$ are in excellent agreement with the experimental data. The average absolute deviations from experiment are only 0.05 eV, and the maximum deviations are 0.10 eV. (3) The accordance between the experimental PES and the theoretical simulations indicates that the ground state structures of $PrSi_n^-$ ($n = 4$–9) reported in this paper are trustworthy. (4) The DEs of Pr atom from $PrSi_n$ species and their anions are larger than those of Eu and Sm. (5) HOMO–LUMO gaps reveal that doping Pr atom to Si_n ($n = 3$–9) species raises the photochemical sensitivity. But the effect of raising photochemical sensitivity is not as good as the effect of the doping Eu or Sm to silicon species. (6) Calculations of magnetic moments show that Pr atom contributes a large proportion of the total magnetic moments.

Acknowledgements We thank Prof. Kit H. Bowen for providing the clear experimental PES of $PrSi_n$ ($n = 4$–9). This work was supported by the National Natural Science Foundation of China (Grant No. 21263010), by Program for Innovative Research Team in Universities of Inner Mongolia Autonomous Region (Gran No. NMGIRT-A1603), and by the Inner Mongolia Natural Science Foundation (Grant No. 2015MS0216).

References

1. Grubisic A, Ko YJ, Wang HP, Bowen KH (2009) Photoelectron spectroscopy of lanthanide–silicon cluster anions $LnSi_n^-$ ($3 \le n \le 13$; Ln = Ho, Gd, Pr, Sm, Eu, Yb): prospect for magnetic silicon-based clusters. J Am Chem Soc 131:10783–10790
2. Grubisic A, Wang HP, Ko YJ, Bowen KH (2008) Photoelectron spectroscopy of europium-silicon clusters anions, $EuSi_n^-$ ($3 \le n \le 17$). J Chem Phys 129:054302-1–054302-5
3. Ohara M, Miyajima K, Pramann A, Nakajima A, Kaya K (2002) Geometric and electronic structures of terbium–silicon mixed clusters ($TbSi_n$; $6 \le n \le 16$). J Phys Chem A 106:3702–3705
4. Koyasu K, Atobe J, Furuse S, Nakajima A (2008) Anion photoelectron spectroscopy of transition metal- and lanthanide metal-silicon clusters: MSi_n^- ($n = 6$–20). J Chem Phys 129:214301-3–214301-7
5. Kenyon AJ (2005) Erbium in silicon. Semicond Sci Technol 20:R65–R84
6. Zhao RN, Han JG (2014) Geometrical stabilities and electronic properties of Si_n ($n = 12$–20) clusters with rare earth holmium impurity: a density functional investigation. RSC Adv 4:64410–64418
7. Zhao GF, Sun JM, Gu YZ, Wang YX (2009) Density-functional study of structural, electronic, and magnetic properties of the $EuSi_n$ ($n = 1$–13) clusters. J Chem Phys 131:114312-1–114312-7
8. Xu W, Ji WX, Xiao Y, Wang SG (2015) Stable structures of $LnSi_6^-$ and $LnSi_6$ (Ln = Pr, Eu, Gd, Tb, Yb), C2v or C5v? Explanation of photoelectron spectra. Comput Theor Chem 1070:1–8
9. Li CG, Pan LJ, Shao P, Ding LP, Feng HT, Luo DB, Liu B (2015) Structures, stabilities, and electronic properties of the neutral and anionic Si_nSm^{λ} ($n = 1$–9, $\lambda = 0, -1$) clusters: comparison with pure silicon clusters. Theor Chem Acc 134:34-1-11
10. Zhao RN, Ren ZY, Guo P, Bai JT, Zhang CH, Han JG (2006) Geometries and electronic properties of the neutral and charged rare earth Yb-doped Si_n ($n = 1$–6) clusters: a relativistic density functional investigation. J Phys Chem A 110:4071–4079
11. Zhao RN, Han JG, Bai JT, Liu FY, Sheng LS (2010) A relativistic density functional study of Si_n ($n = 7$–13) clusters with rare earth ytterbium impurity. Chem Phys 372:89–95
12. Zhao RN, Han JG, Bai JT, Liu FY, Sheng LS (2010) The medium-sized charged $YbSi_n^{\pm}$ ($n = 7$–13) clusters: a relativistic computational investigation. Chem Phys 378:82–87
13. Cao TT, Zhao LX, Feng XJ, Lei YM, Luo YH (2009) Structural and electronic properties of $LuSi_n$ ($n = 1$–12) clusters: a density functional theory investigation. J Mol Struct TheoChem 895:148–155
14. Liu TG, Zhang WQ, Li YL (2014) First-principles study on the structure, electronic and magnetic properties of $HoSi_n$ ($n = 1$–12, 20) clusters. Front Phys 9:210–218
15. Cao TT, Feng XJ, Zhao LX, Liang X, Lei YM, Luo YH (2008) Structure and magnetic properties of La-doped Si*n* ($n = 1$–12, 24) clusters: a density functional theory investigation. Eur Phys J D 49:343–351
16. Peng Q, Shen J (2008) Growth behavior of $La@Si_n$ ($n = 1$–21) metal-encapsulated clusters. J Chem Phys 128:084711-1-11
17. Liu TG, Zhao GF, Wang YX (2011) Structural, electronic and magnetic properties of $GdSi_n$ ($n = 1$–17) clusters: a density functional study. Phys Lett A 375:1120–1127
18. Xie XH, Hao DS, Yang JC (2015) Ytterbium doped silicon clusters $YbSi_n$ ($n = 4$–10) and their anions: structures, thermochemistry, and electron affinities. Chem Phys 461:11–19
19. Xie XH, Hao DS, Liu YM, Yang JC (2015) Samarium doped silicon clusters $SmSi_n$ ($n = 3$–10) and their anions: structures, thermochemistry, electron affinities, and magnetic moments. Comput Theor Chem 1074:1–8
20. Yang JC, Wang J, Hao YR (2015) Europium-doped silicon clusters $EuSi_n$ ($n = 3$–11) and their anions: structures, thermochemistry, electron affinities, and magnetic moments. Theor Chem Acc 134:81-1-11
21. Becke AD (1993) Density-functional thermochemistry. III. The role of exact exchange. J Chem Phys 98:5648–5652
22. Lee C, Yang W, Parr RG (1988) Development of the Colle-Salvetti correlation-energy formula into a functional of the electron density. Phys Rev B 37:785–789

23. Adamo C, Barone V (1999) Toward reliable density functional methods without adjustable parameters: the PBE0 model. J Chem Phys 110:6158–6170
24. Schwabe T, Grimme S (2006) Towards chemical accuracy for the thermodynamics of large molecules: new hybrid density functionals including non-local correlation effects. Phys Chem Chem Phys 8:4398–4401
25. Woon DE, Dunning TH Jr (1993) Gaussian basis sets for use in correlated molecular calculations. III. The atoms aluminum through argon. J Chem Phys 98:1358–1371
26. Cao X, Dolg M (2002) Segmented contraction scheme for small-core lanthanide pseudopotential basis sets. J Mol Struct Theochem 581:139–147
27. Buchachenko AA, Chalasiński G, Szcześniak MM (2007) Diffuse basis functions for small-core relativistic pseudopotential basis sets and static dipole polarizabilities of selected lanthanides La, Sm, Eu, Tm and Yb. Struct Chem 18:769–772
28. Frisch MJ, Trucks GW, Schlegel HB, Scuseria GE, Robb MA, Cheeseman JR, Scalmani G, Barone V et al (2010) Gaussian 09 revision C.01. Gaussian Inc., Wallingford
29. Zhang J, Dolg M (2015) ABCluster: the artificial bee colony algorithm for cluster global optimization. Phys Chem Chem Phys 17:24173–24181
30. Dolg M, Stoll H, Savin A, Preuss H (1989) Energy-adjusted pseudopotentials for the rare earth elements. Theor Chim Acta 75:173–194
31. Dolg M, Stoll H, Preuss H (1993) A combination of quasirelativistic pseudopotential and ligand field calculations for lanthanoid compounds. Theor Chim Acta 85:441–450
32. Yang JC, Xu WG, Xiao WS (2005) The small silicon clusters Si_n (n = 2–10) and their anions: structures, themochemistry, and electron affinities. J Mol Struct Theochem 719:89–102
33. Sekiya M, Noro T, Koga T, Shimazaki T (2012) Relativistic segmented contraction basis sets with core-valence correlation effects for atoms $_{57}$La through $_{71}$Lu: Sapporo-DK-nZP sets (n = D, T, Q). Theor Chem Acc 131:124-7-18
34. Noro T, Sekiya M, Koga T (2012) Segmented contracted basis sets for atoms H through Xe: Sapporo-(DK)-nZP sets (n = D, T, Q). Theor Chem Acc 131:112-4-18
35. Tozer DJ, Handy NC (1998) Improving virtual Kohn-Sham orbitals and eigenvalues: application to excitation energies and static polarizabilities. J Chem Phys 109:10180–10189
36. Sporea C, Rabilloud F, Cosson X, Allouche AR, Frécon M (2006) Theoretical study of mixed silicon-lithium clusters SinLip(+) ($n = 1–6$, $p = 1–2$). J Phys Chem A 110:6032–6038